Extraction of 3D Images Using Pitch-Actuated 2D Laser Range Finder for Robotic Vision

Pinhas Ben-Tzvi

Robotics and Mechatronics Lab
Department of Mechanical and Aerospace Engineering
The George Washington University
Washington, DC, USA
bentzvi@gwu.edu

Samer Charifa

Computer Sciences Corporation
Alexandria, VA, USA

Michael Shick

Department of Computer Science
The George Washington University
Washington, DC, USA

Abstract—**Volumetric mapping is essential for recognizing the 3D environment and consequentially for the decision making process for special-task mobile robots (such as stair climbing, inspection, or search and rescue). In this paper, we propose a fast surface detection algorithm based on point cloud data from a small pitch-actuated laser range finder mounted on a mobile manipulator arm. The developed algorithm is mainly composed of two steps: (i) gradient based classification; and (ii) Recursive Connected Component Labeling (RCCL) algorithm. The algorithm was experimentally validated. A complete segmentation of different planes in the environment was also successfully accomplished.**

Keywords–Robotic vision, laser range finder, 3D environment recognition.

I. INTRODUCTION

Research in robotic motion planning has been focused on using sensor information to build a 2D map of the environment in order to perform obstacle avoidance and localization. Typically, a 2D map is a reasonable approximation for wheeled or tracked robots performing on flat grounds. However, if a robot is intended to surmount an obstacle rather than just avoid it, an essential 3D representation of the obstacle is required. A 3D representation of the environment is needed for mobile robots also to perform tasks, such as inspection, search and rescue, ditch crossing, and stair climbing. However, building a 3D volumetric representation of the environment around the robot has been a challenging task for robotics researchers. Four main techniques have been proposed in the literature as follows:

1. Flash Laser Detection and Ranging
2. Binocular stereo vision systems
3. Fixed Laser Range Finders
4. Pitch-Actuated Laser Range Finder

Unlike the conventional 2D Laser Range Finder (LRF), the Flash Ladar can cover the whole environment with multiple laser flashes. Unfortunately, the 3D images of the typical flash Ladar suffer from motion blur, sensitivity to sunlight, and low resolution. Therefore, Flash Ladar sensors cannot fully replace the conventional 2D LRF [1]. 3D mapping can also be performed using two or more LRFs mounted on a mobile robotic platform. In case of using two LRFs, one is mounted vertically and the other horizontally. By moving the platform, the vertical LRF can scan the surrounding environment and register the readings into a 3D point cloud using the robot's pose. The horizontal scanner is used to compute the robot pose. Unfortunately, this approach suffers from occlusion problems [2]. Implementations of this approach can be found in [3], [4], [5] and [6].

Another method to obtain 3D depth images of the environment around the robot is accomplished by using a Pitch Actuated Laser Range Finder (PALRF). The PALRF technique uses a 2D laser range finder mounted on an actuator that rotates around an axis perpendicular to the direction of interest. At each angle increment, the laser range finder registers the depth information of a single line scan as a vector. These vectors will then be projected onto a local coordinate system that results in a 3D image. This process will be further explained in the rest of this paper.

Surmann et al. [7], [8] have used a PALRF mounted on a mobile robotic platform used to carry tools in a workshop. They proposed an algorithm for surface detection based on integrating the lines of the line detection algorithm to compose surfaces. The problem of this method is that it is sensitive to error because any line-detection error will result in an error in the surface-detection process. Recently, Birk et al. [9] have used a PALRF for 3D perception on a space exploration robotic platform. They have used approximate least-squares technique to solve the plane fitting problem. In [7-9] the PALRF is mounted on a fixed place on the robot, which limits the field of view of the PALRF.

In this paper, we propose a surface detection algorithm using a PALRF. The proposed algorithm is fast $O(n^2)$. Several experiments were carried out to test the 3D vision capability of the LRF system.

II. ROBOTIC DESIGN

The PALRF sensor will be used as the main vision sensor for the Hybrid Mechanism Mobile Robot (HMMR) [10-12] a model of which is shown in Fig. 1. It is a second generation hybrid mobile robot platform that is currently being manufactured. It has a hybrid capability in terms of its ability to use its articulated links for locomotion and manipulation interchangeably [13].

The location of the PALRF will be on the third link, as shown in Fig. 2. Similar to camera in hand principle, this design can be called "Laser in hand" because this will provide an accurate feedback control system for the location of the gripper. Moreover, this design will provide the robot with the ability to obtain a 3D image of the environment from two different locations, which will drastically reduce the occlusion problem. In this paper, we show the testing results of the PALRF, which is mounted on a servo motor, whereas the final mounting of the PALRF would be on the HMMR as shown in Fig. 2.
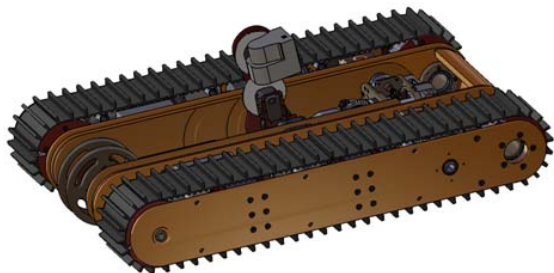

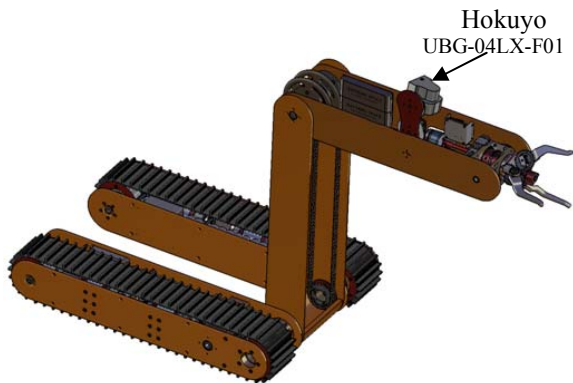Figure 1. The robot with the PALRF scanning on the base link

Figure 2. The PALRF scanning when the third link is deployed

III. PRE-PROCESSING

A. Projection

Every point in the point cloud data of the PALRF can be represented in terms of three variables (ρ, ψ, θ) (see Fig. 3), where ρ is the distance from the LRF to the position of the point of interest, θ is the pitch angle, and ψ is the yaw angle. For every pitch angle θ_i, the values of the 2D polar variables (ρ,ψ) readings of the LRF are projected into a local coordinate

system (x, y, z), (note that z = 0). The origin of this coordinate system is located at the LRF. Since the LRF scanner is rotating, all points in the space will be projected into one LRF coordinate system. We have chosen the location of the LRF coordinate system (X, Y, Z) at the center of rotation, as shown in Fig. 3. The homogenous transformation will transfer any point $P = [P_\rho, P_\psi, P_\theta]^T$ represented using the variables (ρ_i ψ_i, θ_i), into the global coordinates (P_X, P_Y, P_Z). This transformation is described in the following equation:

$$\begin{bmatrix} P_X \\ P_Y \\ P_Z \\ 1 \end{bmatrix} = \begin{bmatrix} 1 & 0 & 0 & 0 \\ 0 & \cos\theta_i & -\sin\theta_i & d\sin\theta_i \\ 0 & \sin\theta_i & \cos\theta_i & d\cos\theta_i \\ 0 & 0 & 0 & 1 \end{bmatrix} \begin{bmatrix} \rho_i\cos\psi_i \\ \rho_i\sin\psi_i \\ 0 \\ 1 \end{bmatrix} \quad (1)$$

where d is the length of the rotating arm as can be seen in Fig. 3. Eq. (1) maps every point in the point cloud into a point in the global coordinate system.
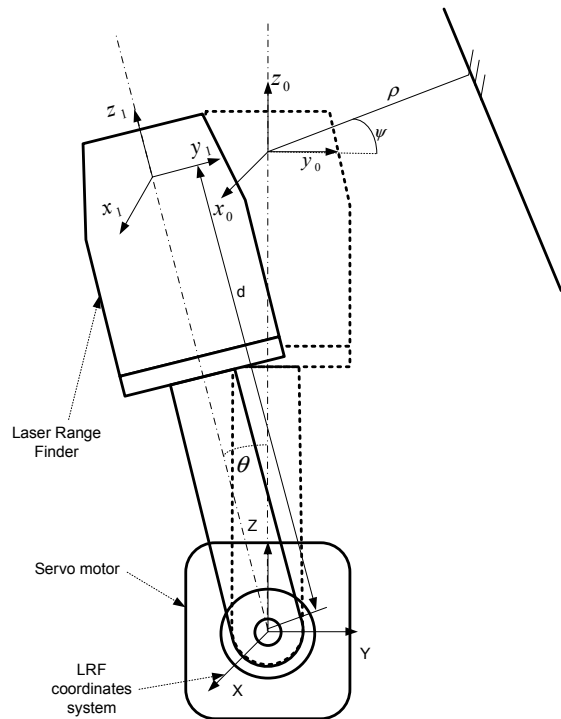

Figure 3. The coordinate system of the LRF experiment

B. Lidar Calibration

It was observed that the percentage error in the LRF reading changes significantly with changes in the pitch angle. This is due to the fact that when the LRF is tilted, the average laser beam signal will be un-calibrated.

In the following experiment the reading of the LRF is taken for a flat surface parallel to the ground. Fig. 4 shows a comparison of the actual and the measured reading of the

PALRF. The x-axis represents the pitch angle of the PALRF. In Fig. 4, the error rate of the measured readings compared to the actual readings is plotted in terms of the pitch angle. It can be noted from the figure that the error rate is more than 35% for small tilting angles. Using Total Least-Squared Regression technique, the cubic polynomial that can approximate the error rate in terms of the pitch angle was found. The equation of the cubic polynomial can be written as:

$$r(\theta) = p_1\theta^3 + p_2\theta^2 + p_3\theta + p_4 \qquad (2)$$

where θ represents the pitch angle, r represents the percentage error rate, and p_i are the polynomial coefficients. The values of the polynomial coefficients are: $p_1 = -1.6221e - 5$, $p_2 = 0.00186$, $p_3 = -0.06264$, and $p_4 = 0.56794$.
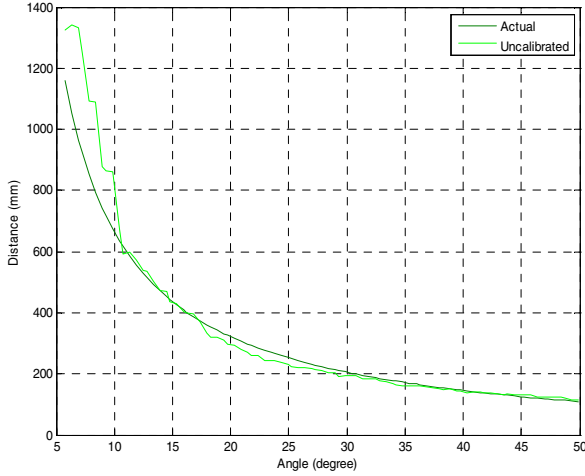

Figure 4. Measured reading of the tilted LRF compare to the actual distances

After calibrating all the data from the PALRF using Equation (2), the percentage error was significantly improved as shown in Fig. 5. The maximum error rate has been dropped from 35% to 15%. This can be seen clearly in Fig. 6.
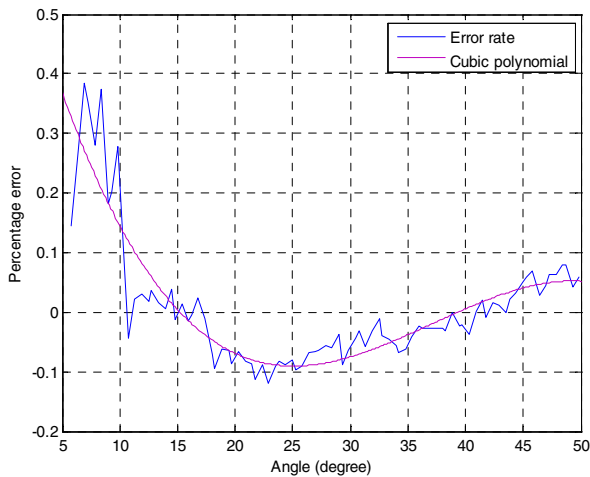

Figure 5. Error rate of the PALRF vs. pitch angle

C. Pre-Filtering

Since the LRF is sensitive to dark colors after a certain range, a high-pass filter is needed to remove the error found in the data (the dark colors will be reflected as very close objects). In this work, we have used a max function with a 9x9 kernel to filter out the distance values that are less than d.
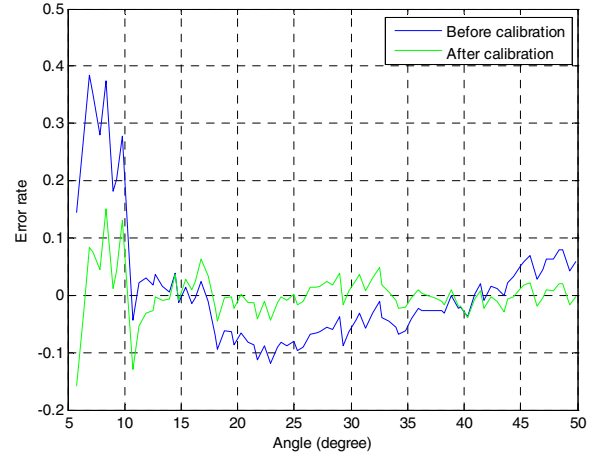

Figure. 6. A comparison of the percentage error rate of the PALRF before and after calibration

IV. SEGMENTATION

Segmentation is a very important feature for 3D environment recognition. Using the following segmentation technique, every surface in the scene around the robot will be labeled and classified. The plane fitting algorithm is divided into the following five steps:

- Compute the gradient of every pixel
- Classify the image based on gradient level
- Convert classified images into binary images
- Apply recursive connected component labeling (RCCL) algorithm
- Post-process to reduce the error

A. Gradient computation

Several techniques are proposed to approximately compute the gradient of a pixel. In this paper, we have used a Sobel operator, which can be represented as:

$$G_x = \begin{bmatrix} 1 & 0 & -1 \\ 2 & 0 & -2 \\ 1 & 0 & -1 \end{bmatrix} * D, \quad \text{and} \quad G_y = \begin{bmatrix} 1 & 2 & 1 \\ 0 & 0 & 0 \\ -1 & -2 & -1 \end{bmatrix} * D,$$

$$G = \sqrt{G_x^2 + G_y^2},$$

where D is the depth map represented by the Y-coordinate of the point cloud, and $*$ represents 2D convolution.

B. Classification

In this step, a simple gradient-based classifier is used to classify the depth map into different levels. The levels of the high gradient values will represent the edges and the ground, as will be shown in the results Section VI.

C. Binary image

The gradient-based image is converted into a binary image using a specified threshold. This is to reflect the change in the gradient in order to capture the edges. The purpose of converting the gradient images into binary images is to "isolate" each surface by its edges.

D. RCCL algorithm

The goal of this technique is to recognize connected areas in the binary images and label them. The algorithm starts by negating the binary image. Then, the algorithm will find a legal neighbor (4-neighbor or 8-neighbor) with the same negative value. After finding all legal connected neighbors, they are labeled, and the process continues to a different label. A detailed explanation of this algorithm can be found in [14].

E. Post processing

The post processing steps are outlined as follows:

- Compute the equation of the surface describing each plane, $Ax+By+Cz+D=0$, using Cramers' rule:

$$A = \begin{bmatrix} 1 & y_1 & z_1 \\ 1 & y_2 & z_2 \\ 1 & y_3 & z_3 \end{bmatrix}, \qquad B = \begin{bmatrix} x_1 & 1 & z_1 \\ x_2 & 1 & z_2 \\ x_3 & 1 & z_3 \end{bmatrix}$$

$$C = \begin{bmatrix} x_1 & y_1 & 1 \\ x_2 & y_2 & 1 \\ x_3 & y_3 & 1 \end{bmatrix}, \qquad D = \begin{bmatrix} x_1 & y_1 & z_1 \\ x_2 & y_2 & z_2 \\ x_3 & y_3 & z_3 \end{bmatrix}.$$

- Find the neighboring planes
- If the neighboring planes have the same equation and the same distance to the PALRF, then merge the two surfaces together

It should be noted here that only flat surfaces are considered in the application of this method in this paper. However, this framework can be extended to non-flat surfaces by modifying the gradient threshold (step C) in order to capture the edges of other surfaces.

V. EXPERIMENTAL SETUP

Several experiments were carried out to test the segmentation algorithm applied on a 3D image of the PALRF system. The PALRF system that was constructed for testing is shown in Fig. 7.

A. Setup

The experiments were carried out with a Hokuyo UBG-04LX-F01 scanning LRF and a Dynamixel RX-28 servomotor. The LRF is implemented with a 785nm Class 1 laser beam with a maximum effective range of 5.6 meters. Distances are measured in a single line of scan over a range of 240 degrees – at the elevation where the laser is positioned – with an angular resolution of 0.36° [15]. The LRF was

actuated with Dynamixel servomotor that draws a maximum current of 1200 mA at 14.4 V. The Field of View (FOV) used for this experiment was (70°x50°) with a resolution of 0.29° vertically and 0.35° horizontally, which means that the FOV matrix is (147x210). The scanning time required to cover the whole FOV is 4 seconds.
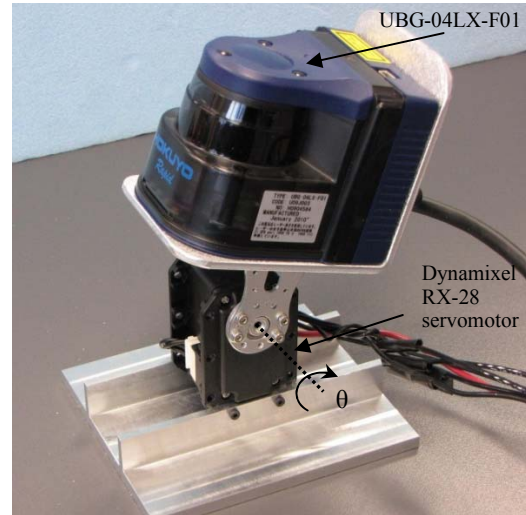

Figure 7. Experimental setup of a pitch-actuated laser range finder

B. Communication

Both the range finder and servomotor operate over serial connections. The servomotor uses RS485 and the range finder uses ACM serial over USB by the Communication Device Class specification. Commands are transmitted to both units over their respective serial connections, and data is acquired as an ASCII bit stream from the range finder for processing in the computer.

VI. EXPERIMENTAL RESULTS

The environment shown in Fig. 8 was created to test the segmentation algorithm on the PALRF data. It is composed of a ground table, three stairs with different heights, small area to the left with high depth, and a background.
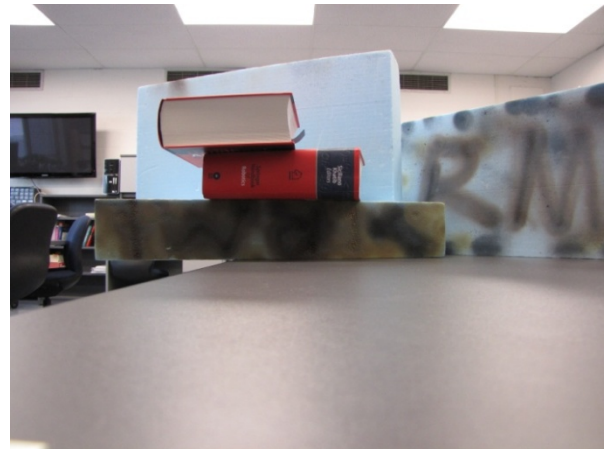

Figure 8. Testing environment

When projecting the data into 3D space using the projection described in Equation (1), a 3D data image can be obtained, as shown in Fig. 9. This figure shows the contour plots of the (X,Y,Z) data of the 3D point cloud. This provides a reconstruction of the full scene based on the gradient.
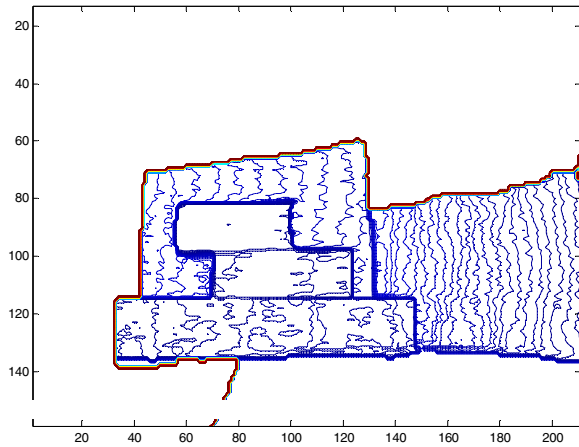

Figure 9. A contour plot of the projected point cloud

The next step is to classify the 3D cloud based on the gradient and the depth (distance) estimate. In order to recognize the edge of each surface, the threshold of the gradient difference is considered to be to be 30 [mm]. This seems to be reasonable for this type of applications.

The results shown in Fig. 10 indicate that the three steps have the same gradient value. The background, the ground table, and the right side area all have different gradient levels. Clearly, the algorithm was able to differentiate between the background, the steps and the ground. In the following steps, the developed algorithm demonstrates its ability to detect each plane separately.

Figure 10. The testing environment is plotted with different levels of gradient and depth

In the next step, the image was converted into a binary format, as shown in Fig. 11.
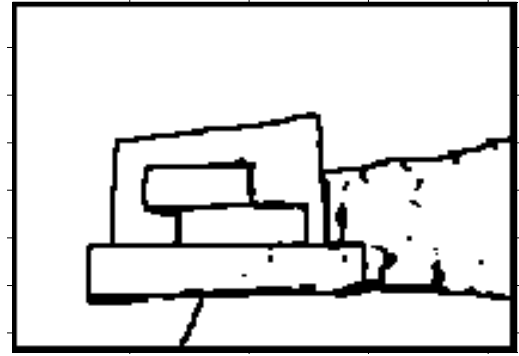

Figure.11. Image converted into a binary format

In the last step, the recursive component labeling algorithm is applied to the binary image. As can be seen from Fig. 12, the results are very satisfactory. All the different planes in the environment were successfully labeled with different colors (colors were used just for illustration purposes) – namely, the environment has been classified into regions. Minor errors can be seen in the corners; however, the classification process was successfully accomplished.
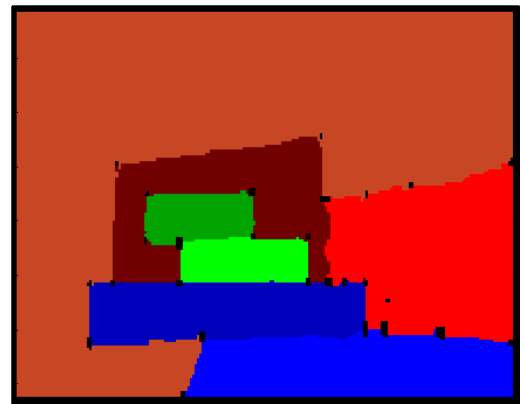

Figure 12. The final step showing a complete recognition of different planes in the testing environment

Figs. 13 and 14 show another environment that has been tested. The tested 3D segmentation shows clearly that every surface was labeled with a different color. It should be noted that in cases where the gradient level is high in the same surface (typically represents sloped surfaces), the post-processing step is very important for detecting the equation of each surface and then merging them together.
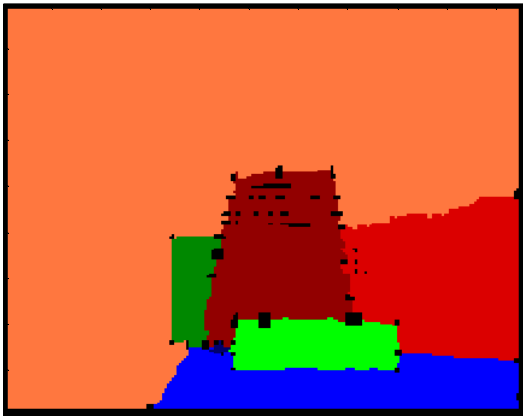
Figure 13. An additional testing environment

Figure 14. Segmentation results of the additional environment

VII. CONCLUSIONS

In this paper, we have tested a 3D environment recognition algorithm on data obtained from a pitch actuated laser range finder. This data was filtered and projected into a 3D Euclidean space. Then, the data was classified using a gradient-based classifier. After converting the data into binary image, the RCCL algorithm was applied in order to label the connected areas. As a result, every plane in the environment was separately labeled. The testing results show that the labeling algorithm was successfully able to recognize different planes in the 3D environment.

As the next step, we plan on installing this pitch-actuated laser range finder along with the developed algorithm on a hybrid mechanism mobile robotic system that has been designed to autonomously climb large obstacles, rubble-pile, steps, stairs, etc. This algorithm will greatly help with identifying and distinguishing between different obstacles and make proper measurements in real-time (distance to objects, dimensions of objects, etc) in order for the robot to semi-autonomously execute the required link motions to complete obstacle climbing effectively.

ACKNOWLEDGMENT

REFERENCES

[1] D. Anderson, H. Herman, and A. Kelly, "Experimental Characterization of Commercial Flash Ladar Devices," *International Conference of Sensing and Technology*, Palmerston North, New Zealand, Nov. 2005, pp. 17-22.

[2] H. Zhao, R. Shibasaki, "Reconstructing textured CAD model of urban environment using vehicle-borne laser range scanners and line cameras", *Proceedings of the Second International Workshop on Computer Vision System (ICVS'01)*, Vancouver, Canada, July 2001, pp. 284–295.

[3] S. Thrun, D. Fox, and W. Burgard, "A real-time algorithm for mobile robot mapping with application to multi-robot and 3D mapping," *IEEE International Conference on Robotics and Automation (ICRA'00)*, San Francisco, CA, April 2000.

[4] D. Hahnel, W. Burgard, and S. Thrun, "Learning Compact 3D Models of Indoor and Outdoor Environments with a Mobile Robot", *Robotics & Autonomous Sys.*, vol. 44, pp. 15-27, 2003.

[5] A. Howard, D.F. Wolf and G.S. Sukhatme, "Towards 3D Mapping in Large Urban Environments," *IEEE/RSJ International Conference on Intelligent Robots and Systems (IROS)*, Sendai, Japan, Sep 2004, pp. 419-424.

[6] M. Montemerlo and S. Thrun, "Large-scale robotic 3d mapping of urban structures," *in 9th International Symposium on Experimental Robotics*, Singapore, June, 2006, pp. 141-150.

[7] H. Surmann, A. Nüchter, and J. Hertzberg, "An autonomous mobile robot with a 3D laser range finder for 3D exploration and digitalization of indoor environments" *Robotics and Autonomous Systems*, vol. 45, Sep. 2003, pp. 181–198.

[8] H. Surmann, K. Lingemann, A. Nüchter, J. Hertzberg, "Fast acquiring and analysis of three-dimensional laser range data," *Proceedings of the Sixth International Fall Workshop Vision, Modeling, and Visualization (VMV'01)*, Stuttgart, Germany, Nov. 2001, pp. 59-66.

[9] A. Birk, N. Vaskevicius, K. Pathak, S. Schwertfeger, J. Poppinga, and H. Buelow, "3-D perception and modeling," *IEEE Robotics and Automation Magazine*, vol. 16, Dec. 2009, pp. 53-60.

[10] P. Ben-Tzvi, "Experimental Validation and Field Performance Metrics of a Hybrid Mobile Robot Mechanism", J. Field Robotics, Vol.27, No. 3, pp. 250 – 267, 2010.

[11] P. Ben-Tzvi, A.A. Goldenberg, J.W. Zu, "Design and Analysis of a Hybrid Mobile Robot Mechanism with Compounded Locomotion and Manipulation Capability", Transactions of the ASME, J. Mechanical Design, Vol.130, pp. 1 – 13, 2008.

[12] P. Ben-Tzvi, A.A. Goldenberg, J.W. Zu, "Design, Simulations and Optimization of a Tracked Mobile Robot Manipulator with Hybrid Locomotion and Manipulation Capabilities", Proceedings of the 2008 IEEE International Conference on Robotics and Automation (ICRA2008), California, pp. 2307 – 2312, 2008.

[13] P. Ben-Tzvi, A.A. Goldenberg, J.W. Zu, "Articulated Hybrid Mobile Robot Mechanism with Compounded Mobility and Manipulation and On-Board Wireless Sensor/Actuator Control Interfaces", J. Mechatronics, Vol.20, No.6, pp. 627 – 639, 2010.

[14] L.G. Shapiro and G.C. Stockman, "*Computer Vision*," Prentice-Hall, NJ, 2001.

[15] H. Kawata, A. Ohya, S. Yuta, W. Santosh, and T. Mori, "Development of ultra-small lightweight optical range sensor system," *International Conference Intelligent Robots and Systems,* (*IROS 2005*)*, Aug. 2005, pp. 1078-1083.